Characteristics Analysis of RFID Multiparameter Sensor Tags Based on Various Substrate Materials

Lei Kang, Lan Chen, Luyi Liu, Zhichong Wan, Guochun Wan, and Liyu Xie

***Abstract*—Not only are large bridges and structures susceptible to structural collapse owing to mechanical loads, but they are also susceptible to structural degeneration due to insufficient environmental monitoring. Therefore, the monitoring of environmental characteristics must be added to the field of structural health monitoring, which is no longer sufficient if it focuses just on changes in mechanical qualities. In this research, a reversible multiparameter sensor for temperature and humidity detection is developed so that it can be reused to increase economic efficiency. A portable, low-cost vector network analyzer (VNA) is used to detect the change in temperature and humidity by observing the shift of the resonant frequency of the sensor, and the performance of a multiparameter sensor with various substrates is compared and assessed The humidity sensitivity of the sensor is about 1.8 MHz/RH. A linear fit using normalized frequency shift with temperature results in greater temperature sensitivity of 179.23 ppm/°C for the RO3010, proving the sensor's viability. In addition to identifying various sensors, a 5-bit resonator tag was created for coded identification.**

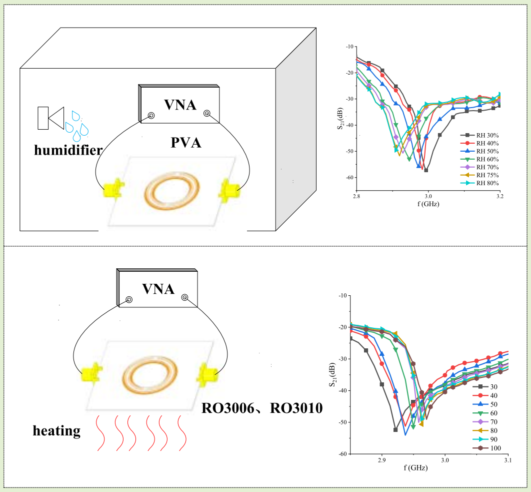

***Index Terms*—Humidity sensors, multiparameter sensors, radio-frequency identifier (RFID) tag, structural health monitoring, temperature.**

I. INTRODUCTION

CIVIL infrastructures such as bridges and buildings are susceptible to disaster causes such as severe environmental degradation and long-term impacts of loads, which can result in infrastructure deterioration and cause serious accidents pertaining to social and economic difficulties. Using sensing technologies to assess the system of bridges and building structures, structure health monitoring (SHM) is used to monitor structural damage or degradation to prevent loss of socioeconomic and human life. Passive radio-frequency identifier (RFID) technology enables distributed structural health monitoring because of its low cost, passive wireless, and long reading distance characteristics [1]. Currently, researchers are focused not only on structural health monitoring in the study of mechanical properties, but also on the physical factors of the structure's environment, such as temperature, humidity, pH, and other parameters [2], [3].

The interaction of environmental physical elements with RFID sensors generates changes in the dielectric constant of the sensitive material, resulting in a shift in the resonant frequency and a change in the amplitude of the sensor cells [4]. The first technique is to use the sensing material as a substrate [5], [6]; when the surrounding environmental factors change, the dielectric constant of the substrate changes, leading to changes in parameters such as the resonant frequency of the sensor. The second step involves coating the sensor with a sensing substance, which alters properties such as the resonant frequency [7], [8].

Temperature is a crucial indicator for monitoring the structural health of a bridge. In the summer, the temperature of

Manuscript received 17 November 2022; accepted 12 December 2022. Date of publication 20 December 2022; date of current version 31 January 2023. This work was supported in part by the General Program of the National Natural Science Foundation of China, in part by the Research on the Principles of Passive Sensing and Structural Deformation Monitoring Methods Based on Antennas Without Stress Patch under Project 52078375, and in part by the Top Discipline Plan of Shanghai Universities-Class I. The associate editor coordinating the review of this article and approving it for publication was Dr. Fathi Abdelmalek. *(Corresponding author: Lan Chen.)*

Lei Kang, Lan Chen, Luyi Liu, and Zhichong Wan are with the Department of Electrical and Electronic Engineering, Shanghai Institute of Technology, Shanghai 201418, China (e-mail: kl0314@163.com; chenlan@sit.edu.cn; 206101113@mail.sit.edu.cn; 206101111@mail.sit.edu.cn).

Guochun Wan is with the Department of Electronic Science and Technology, Tongji University, Shanghai 200092, China (e-mail: wanguochun@tongji.edu.cn).

Liyu Xie is with the Department of Disaster Mitigation for Structures, Tongji University, Shanghai 200092, China (e-mail: liyuxie@tongji.edu.cn).

Digital Object Identifier 10.1109/JSEN.2022.3229467

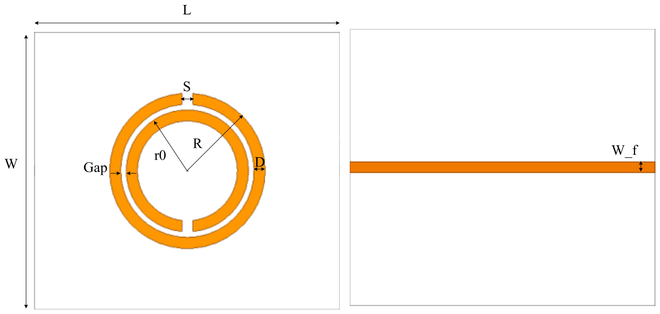

(a) (b)

Fig. 1. Pair of CSRR resonator tags. (a) Top. (b) Bottom.

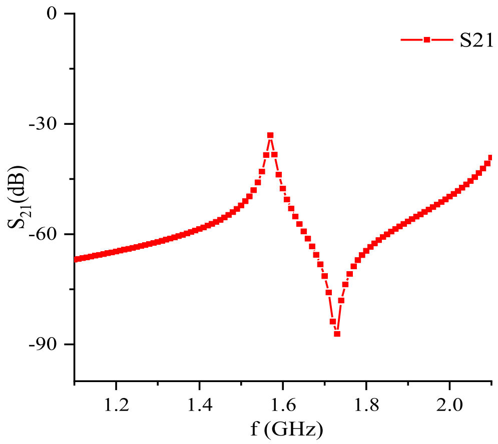

Fig. 2. Simulation results of single resonance on the CSRR resonator tag.

TABLE I
SIZE OF THE SINGLE RESONANT PAIR CSRR RESONATOR TAG

Parameter	W	L	R	D	Gap	W_f	S
Value(mm)	50	60	14	2	1	2	2

the bridge deck can approach 60 °C, which is approximately 20 °C higher than the air temperature. The bridge structure can be deformed by high temperatures [9]. RFID tags are utilized as temperature sensors to monitor the structure's temperature. Athauda and Karmakar [10] proposed a multiparameter sensor that deploys smart materials sensitive to ambient temperature on a substrate, and when the ambient temperature changes, the selected smart materials trigger a change in their dielectric properties based on the presence of specific environmental conditions or threshold levels, resulting in a change in resonant frequency response. Javed et al. [5] presented an RFID multiparameter sensing for mild fracture monitoring in IoT contexts with a substrate of Rogers RT/Duroid[1] 6010.2LM, whose dielectric characteristics change when the temperature fluctuates and so enables temperature monitoring.

Humidity is one of the most important factors influencing the cement maturation process, as it affects cement's stability, hydrate transformation, and strength development. Humidity also affects cement and reinforcement corrosion. Both cement hydration and environmental dryness result in a reduction of free water in the cement matrix, resulting in shrinkage. When the cement matrix is constrained by factors such as reinforcement and aggregates and is unable to shrink freely, it will generate tension and eventually lead to structural cracking [11]. Consequently, moisture monitoring is important for bridges as well. Ahmad et al. [12] presented a sensor for soil moisture monitoring based on an interdigital capacitor (IDC) structure that is insensitive to changes in the surrounding dielectric constant, except for a portion of the IDC that is sensitive to such changes. Sensing is based on the change in phase of the input signal's response upon reflection, while its amplitude and phase fluctuate with the change in the dielectric constant of the test medium [12]. Jia et al. [13] suggested a PEDOT, a PSS-based differential humidity sensor for relative humidity (RH) measurement. Three distinct approaches, including the air-filled substrate, metal grid holes (METGH), and sensitive materials, were employed to improve the response of the humidity sensor [13].

Currently, wireless systems are growing toward multifunctionality for quick, secure, and dependable communication, and antennas are one of the major enabling components that play a crucial role in deciding the eventual performance of wireless systems [14]. When there are many antennas in a sensor network, the identifying coding unit is typically appended to the tag, and even if the antennas are colocated, the transmit and receive signals on various antennas can be independently processed and designed. To develop intelligence in antenna systems, the majority of current research employs binary coding for identification by converting 0–1. Wang et al. [15] suggested a wideband dual-polarized binary-coded antenna and its array, in which binary-coded drivers and parasitic patches are used to increase the bandwidth and beamwidth.

The authors developed a reusable temperature and humidity sensor based on a temperature-sensitive substrate in conjunction with the aforementioned research. The sensor is placed in the monitored environment, and changes in the surrounding environmental factors are detected by the shift in the resonant frequency. Multiple substrates are used to compare the sensor's features. On this basis, a 5-bit encoded tag is also devised for multiple antenna identification.

II. DESIGN WITH CSRR STRUCTURE

Rogers RT 3003 was selected for the preliminary resonator tag design in this article. Rogers RT 3003 is a high-frequency circuit material, a ceramic-filled polytetrafluoroethylene (PTFE) composite, utilized largely for commercial microwave and RF applications. It is intended to give superior electrical and mechanical stability to a greater degree [16].

In Fig. 1, the RFID tag designs make use of complementary split-ring resonators (CSRRs). A collection of open resonant rings resembles a small *LC* resonant element circuit, and the connected *LC* forms a current loop within the circuit. Its

---

[1] Registered trademark.

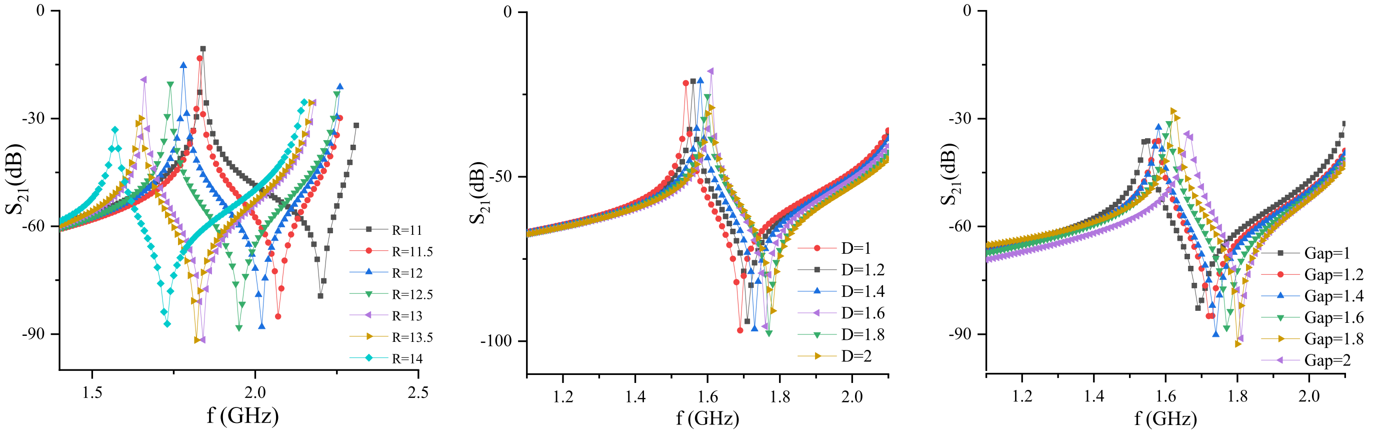

(a) (b) (c)

Fig. 3. Resonant frequency versus antenna size for the CSRR. (a) Results of S_{21} with a different circle radius R. (b) Results of S_{21} with linewidth D. (c) Results of S_{21} with a different circle gap.

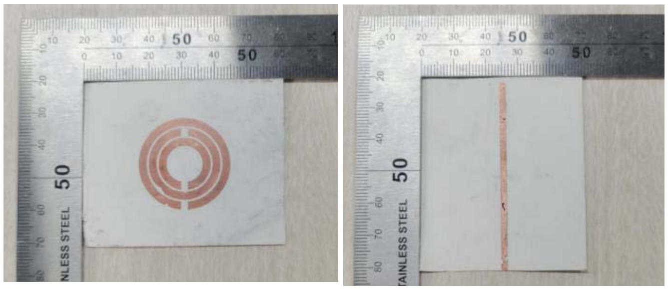

(a) (b)

Fig. 4. 2-bit resonator tag. (a) Top. (b) Back.

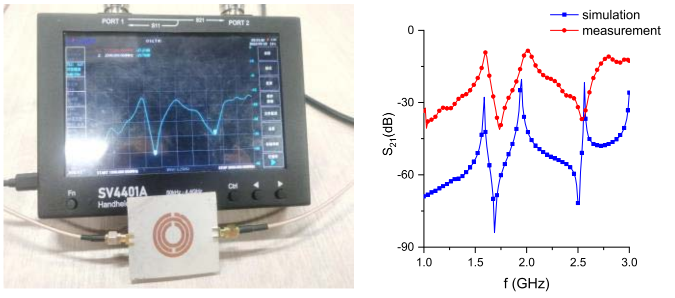

(a) (b)

Fig. 5. (a) Actual tag measurement. (b) Comparison of label simulation and actual measurement results.

resonant frequency is determined by using the following [17]:

$$f=\frac{1}{2\pi\sqrt{L_T C_{eq}}}=\frac{1}{2\pi\sqrt{L_T[\frac{(\pi r_0-S)C_{pul}}{2}+\frac{\varepsilon_r ch}{2S}]}} \quad (1)$$

where f is the frequency, L_T is the resonant cavity equivalent inductance, ε_r is the effective dielectric constant of the medium, $C_{\text{eq}}$is the resonant cavity equivalent capacitance, S is the opening gap of CSRR, C_{pul} is the unit length capacitance, and r_0 between the rings is the distance from the two constituent rings of CSRR to the center. C_{pul} is calculated by the following [17]:

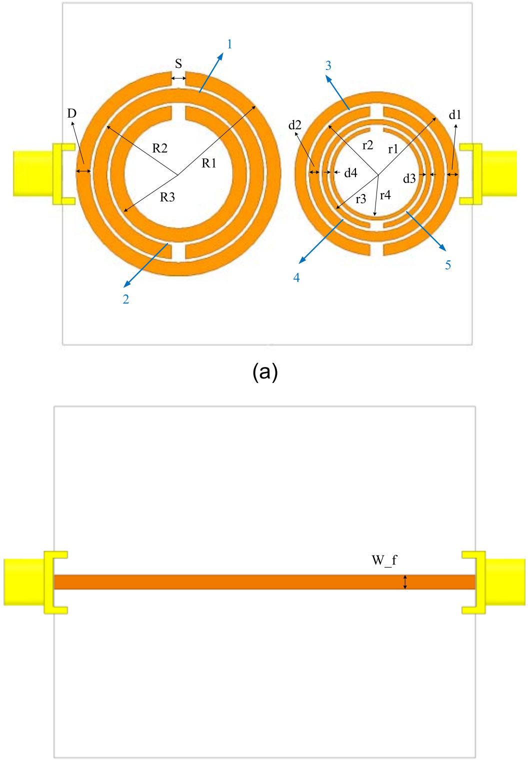

(a)

(b)

Fig. 6. 5-bit tag. (a) Top. (b) Back.

$$C_{\text{pul}}=\frac{\sqrt{\varepsilon_r}}{cZ_0} \quad (2)$$

where $C=3\times10^8$ m/s is the speed of light in free space, ε_r is the effective dielectric constant of the medium, and Z_0 is the impedance of the medium.

The equivalent inductance of the structure was calculated by using the following [17]:

$$L_{\text{eq}} = 0.00508l\left(2.303\log_{10}\frac{4l}{d} - \theta\right) \quad (3)$$

where l and d are the wire length and width, respectively. The constant θ varies with the wire geometry and the CSRR is 2.451.

Microstrip lines are applied to the back of the tag and are used to couple complimentary open resonant rings. By modifying the shape and size of the CSRR, resonator tags are created for different frequency bands. To identify the appropriate scanning parameters for the encoded information utilizing frequency shift techniques, the radius of the CSRR and inner and outer ring parameters are currently being explored. In the parametric research, just one parameter is altered, while the other parameters are held constant based on the prior size requirements, to determine the impact of each parameter on the tag's performance. The influence of each parameter on the frequency of resonance was then examined. The objective is to identify the ideal design of the CSRR structure by altering the parameters, including the miniaturization of the tag and the tuning of the resonant frequency range. The tag is fabricated as illustrated in Fig. 1, and its final dimensions are listed in Table I. Its simulation results are depicted in Fig. 2.

A. Relationship Between Parameter Size and Resonant Frequency

The impacts of circle radius, circle width, and circle split gap on the CSRR transmission coefficient are investigated in this section. The single resonant CSRR tag structure is utilized, and the tag parameters are adjusted independently; the results are depicted in Fig. 3. The outer ring radius is between 11 and 14 mm, and the step size is 0.5 mm. The resonant frequency reduces as the ring radius grows, as shown in Fig. 3(a). However, as shown in Fig. 3(b), when the ring width increases from 1 to 2 mm with a step size of 0.2 mm, the resonant frequency increases. Therefore, when the frequency needs to be decreased, there is no need to increase the radius of the tag, however, reducing the width of the resonator can also achieve the same result, to meet the antenna miniaturization requirements. Lastly, based on the results of the circular gap change Fig. 3(c), it can be concluded that the circular line length of the CSRR also affects the resonant frequency; when the line length is longer, the resonant frequency is lower, indicating that the key parameter affecting the resonant frequency is the radius of the resonant ring, which can be increased by increasing the radius of the resonant ring to achieve a lower resonant frequency.

B. Multibit Encoded Label Design

By increasing the number of open resonant rings, it is possible to increase the LC resonant circuit and hence the number of trapped waves. Each of the three open resonant rings consists of two adjacent groups of resonant circuits, as depicted in Fig. 4(a) for the front side of the 2-bit resonator tag and Fig. 4(b) for the back side of the tag. As illustrated in Fig. 5(a), the tag is manufactured by etching an RO3003 substrate and analyzed using a vector network analyzer (VNA) (SYSJOINT SV4401A). Fig. 5(b) depicts the simulated and measured S_{21} results. Due to the fabrication process, environmental impact, and other aspects, although there is a difference between the two comparisons, the inaccuracy is within the acceptable range, thereby validating the design's viability.

TABLE II
SIZE OF THE 5-bit TAG

Parameter	R1	R2		R3	D	S		W_f
Value(mm)	15	12.5		10	2	2		2
Parameter	r1	r2	r3	r4	d1	d2	d3	d4
Value(mm)	12	9.9	8	6.8	1.6	1.4	0.7	0.5

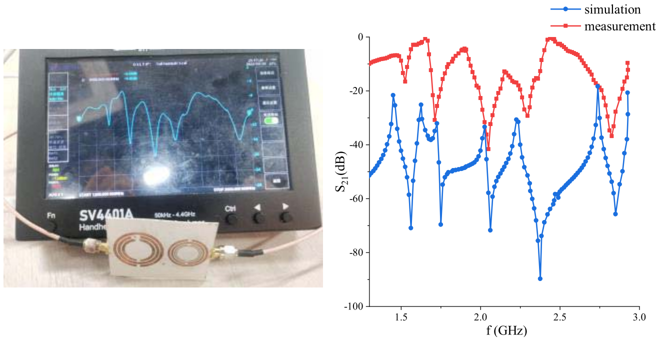

(a) (b)

Fig. 7. (a) Actual tag inspection pictures. (b) Comparison of label simulation and actual measurement results.

This section demonstrates the design of a flexible RFID tag with a 5-bit CSRR based on Rogers RT 3003 substrate, as seen in Fig. 6(a) and (b), and the five resonant cavities are numbered. When the resonant frequency is present, the identification number is specified as 1. When the LC resonant structure is eliminated, the resonant frequency vanishes, and the ID becomes 0. The maximum information carried by a 5-bit RFID tag is $2^5 = 32$ bits. By adding a resonant structure, the amount of information can be enhanced, but in the same frequency range, false codes may occur, making the antenna less dependable.

By further extending the previous design, the number of open resonant rings is increased to increase the number of resonant units and thus the number of bits of encoded information. The spacing between the two outermost open resonant rings reduces the coupling between the two independent structures. The capacitance and inductance are increased by decreasing the width of the right innermost open resonant ring, which in turn reduces the resonant frequency of the innermost ring resonant cavity to minimize the frequency range [18]. The optimal tag size is determined using the high frequency structure simulator (HFSS) optimetrics function, and the final size of the tag is shown in Table II to ensure that there is a certain interval between two adjacent resonant frequencies to avoid overlapping in the same frequency range. Fig. 7(a) shows the actual tag measurements. The simulated

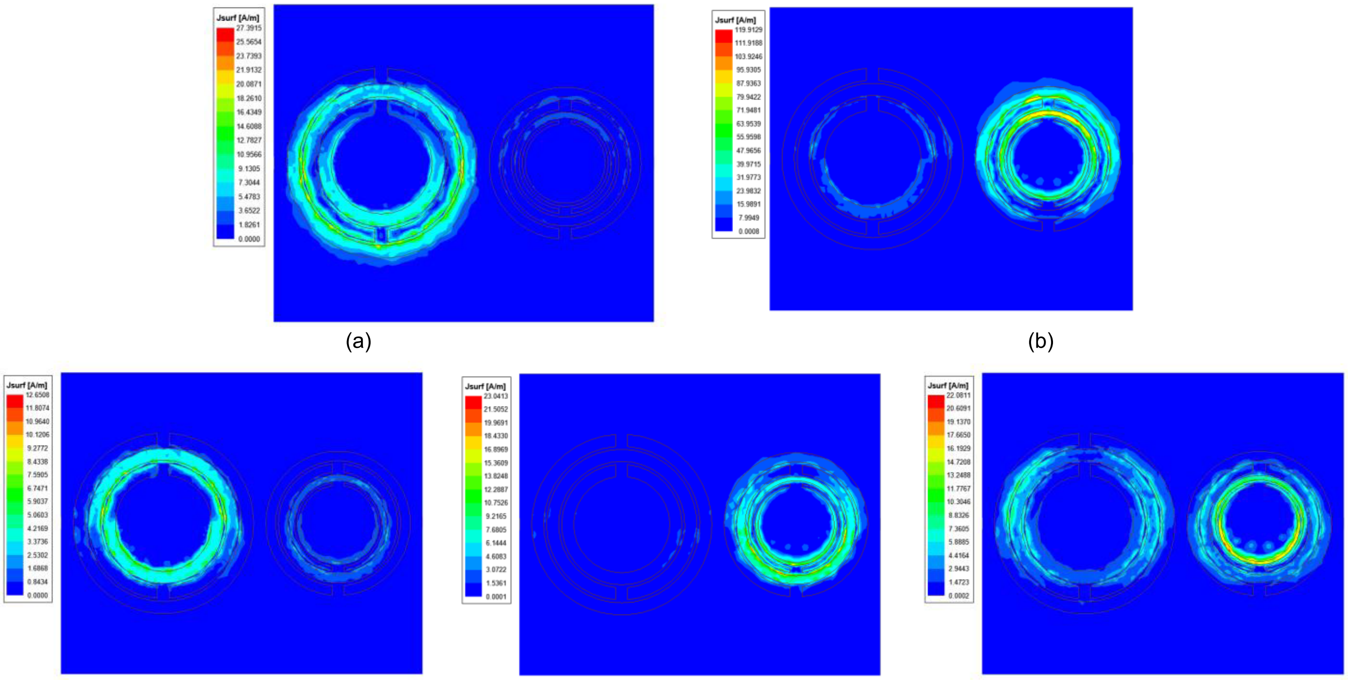

(a) (b)

(c) (d) (e)

Fig. 8. Surface current of a 5-bit tag. (a) 1.55 GHz. (b) 1.72 GHz. (c) 2.06 GHz. (d) 2.27 GHz. (e) 2.81 GHz.

resonant frequencies are shown in Fig. 7(b) as 1.55, 1.72, 2.06, 2.27, and 2.81 GHz, and the S_{21} response curve of the tag after constructing the tag in the lab and measuring it with a VNA. The first resonant cavity corresponds to a resonant frequency of 1.55 GHz, the second resonant cavity corresponds to a resonant frequency of 2.06 GHz, the third resonant cavity corresponds to a resonant frequency of 1.72 GHz, the fourth resonant cavity corresponds to a resonant frequency of 2.27 GHz, and the fifth resonant cavity corresponds to a resonant frequency of 2.81 GHz. The measurement results have some deviation, but the error is within the allowable range due to the low precision of the laboratory fabrication process and the interference of the ambient noise. By analyzing the surface current distribution of the resonant cavity during the simulation process, the electromagnetic behavior can be analyzed [18]. As depicted in Fig. 8, a current flow exists at the resonant frequency in the space between the two rings. According to the current distribution diagram and the theoretical analysis, while the frequency is low, the majority of the current is dispersed in the resonant cavity with a larger radius, and as the frequency increases, the radius of the resonant cavity decreases progressively.

III. TEMPERATURE AND HUMIDITY DETECTION EXPERIMENT

The purpose of this article is to design a sensor with integrated temperature and humidity monitoring. In this section, Rogers RO3006, RO3010, and RO3210 are selected as the tag substrate for temperature-sensing simulation, when the temperature changes, the dielectric constant of the substrate changes and then affects the resonant frequency of the tag. To ensure that the same RFID tag can be combined with multiple physical parameter sensing, the tag between the two rings is filled with intelligent sensing materials, and changes in humidity lead to changes in the dielectric constant, which are then mapped to the resonant frequency of the sensor, and thus humidity monitoring is achieved. The chosen substrate is a flexible substrate that fits well with the structure to be measured and ensures accurate detection.

A. Humidity Detection Experiment

In this article, the resonant cavity of the proposed RFID tag is coated with humidity-sensitive polymeric polyvinyl alcohol (PVA). PVA is a hygroscopic polymer with OH groups that form H–H bonds in the presence of water molecules, and humidity has a dual effect on the electrical properties of PVA. PVA has dielectric and conductive sensitivity in response to changes in humidity; hence, variations in the resonant frequency represent changes in RH [19].

To measure the feasibility of humidity detection of PVA overlay on CSRR structures, we chose the 2-bit tag in Section II for preliminary experiments, dissolved PVA in water, and stirred it, as the dissolution process was slow and contained many air bubbles. To reduce the bubbles, the solution is left for some time until it is completely dissolved to obtain a transparent gel with basically no bubbles. Then the outer resonant ring is filled with PVA solution in the middle and dried completely, as shown in Fig. 9(a). The humidity in the house is high due to the weather, as shown in Fig. 9(b), first, the $CaCl_2$ desiccant is put into the foam box, and a high-precision electronic humidity detector is used for real-time humidity detection. We choose a portable, low-cost VNA, and the coaxial cable connecting the two ends of the label is threaded out of the box through a small hole and connected to the VNA. Finally, the transparent tape is used to seal the

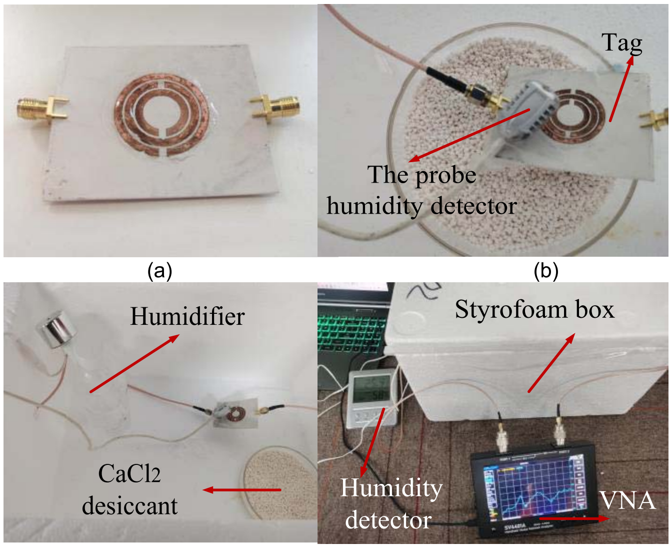

(a) (b)

(c) (d)

Fig. 9. Humidity detection device. (a) 2-bit label filled with PVA solution. (b) Testing device using only $CaCl_2$ desiccant. (c) Testing device with humidifier added. (d) Overall humidity testing device.

box to reduce the interference of the surrounding environment, and the measured data is used as the initial humidity. Next, as shown in Fig. 9(c), a humidifier is placed inside the box, $CaCl_2$ desiccant is added to the box and the box is sealed at the same time to prevent the humidity from rising rapidly. The tags of RO3006 and RO3010 substrates are detected in the same way, with an initial humidity of 30% and an RH setting between 30% and 80%.

Fig. 10(a) and (b) shows the actual measurement data with PVA applied to the outer ring of the RO3003 substrate tag. The frequency of the first trap corresponding to the external resonant cavity is shifted, and the frequency of the second trap corresponding to the internal resonant cavity is almost constant. Fig. 11(a) shows the results of the RO3006 substrate tag and Fig. 11(b) shows the results of the RO3010 substrate tag. From the obtained curves, it can be seen that the resonant frequency gradually decreases and the trap depth gradually decreases with the increase in humidity. Fig. 12 depicts the result of fitting the found relationship between humidity and frequency shift. Although the experimental data are affected by the surroundings and the thickness of the PVA, the overall trend is consistent [20], with high linearity between humidity and frequency offset and a sensitivity of 1.8 MHz/RH on average for the three sensors. This humidity-detecting sensor is reversible and cost-effective because PVA may be returned to its original condition after air-drying.

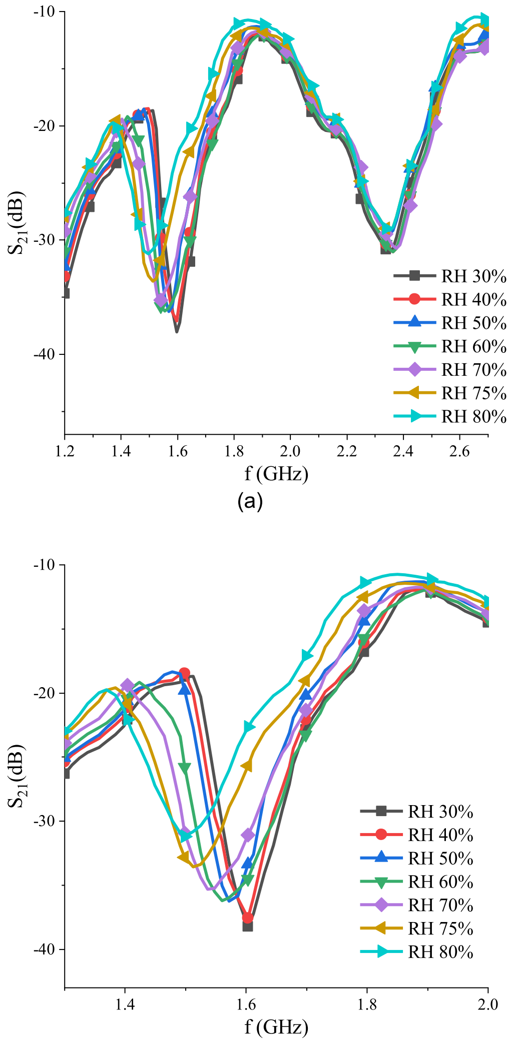

(a)

(b)

Fig. 10. Actual measurement results of 2-bit RO3003 substrate tag results. (a) Shift in frequency of two resonant points. (b) Shift in frequency of the first resonant point.

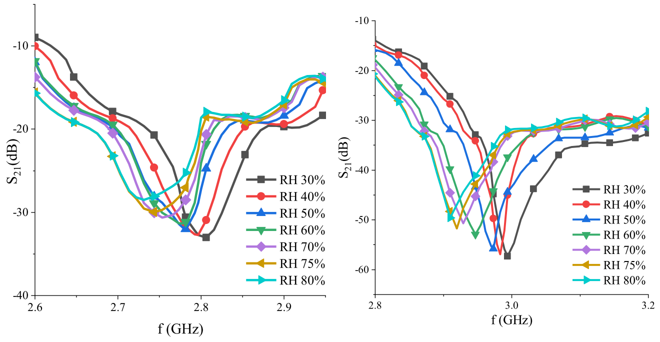

(a) (b)

Fig. 11. Actual measurement results of (a) RO3006 substrate tag result and (b) RO3010 substrate tag result.

B. Temperature Monitoring Simulation and Experiment

The temperature-sensitive substrate is chosen for the tag, and when the temperature changes, the substrate's dielectric constant changes, resulting in a shift in the resonant frequency. The dielectric constant of PVA is almost zero in the higher frequency range and is minimally affected by temperature [21], [22], so this effect is ignored. The offset of the resonant frequency is proportional to the substrate's dielectric constant ε_r and the resonator's length, and the precise link is represented by the following [6], [23]:

$$\delta f = \frac{\partial f}{\partial \varepsilon_r}\delta\varepsilon_r + \frac{\partial f}{\partial L}\delta L. \tag{4}$$

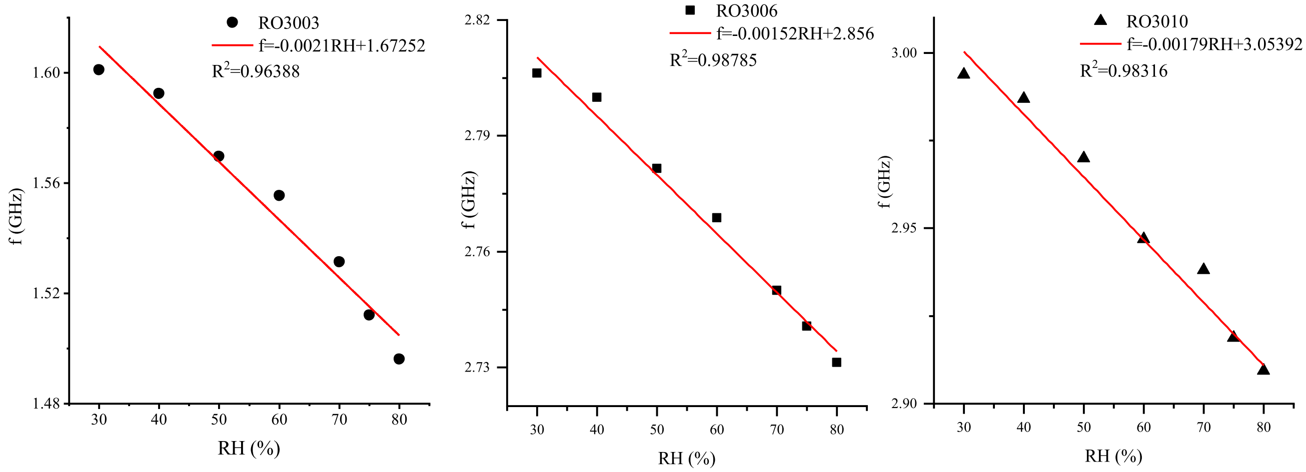

(a) (b) (c)

Fig. 12. Fitting curves for humidity and frequency offset. (a) Fitting curves for RO3003 substrate measurements. (b) Fitting curves for RO3006 substrate measurements. (c) Fitting curves for RO3010 substrate measurements.

(a) (b) (c)

Fig. 13. Temperature sensing tags. (a) Tag for the RO 3006 substrate. (b) Tag for the RO 3010 substrate. (c) Tag for the RO 3210 substrate.

TABLE III
VARIATION OF THE DIELECTRIC CONSTANT

Substrate parameters	RO3006	RO3010	RO3210
Dielectric constant(εr)	6.15	10.2	10.2
Thermal Coefficient(TCDk)	-262	-395	-459
Coefficient of thermal expansion	17	13	13
Temperature sensitivity(kT)	118	184.5	216.5
$\delta\varepsilon_r$	0.03	0.08	0.09
Moisture Absorption	0.02%	0.05%	<0.1%

Normalize the frequency shift of the tag to get by the following [23]:

$$\frac{\partial f}{f} = -\frac{1}{2}\frac{\delta\varepsilon_r}{\varepsilon_r} - \frac{\delta L}{L}. \tag{5}$$

Finally, a linear relationship between the normalized frequency shift and temperature change is established by the following [23]:

$$\frac{\partial f}{f} = -\left(\frac{1}{2}\alpha_\varepsilon + \alpha_T\right)\delta T = k_T \delta T \tag{6}$$

where α_ε is the thermal coefficient of the dielectric constant of the substrate (TCDk), and the sensitivity of the resonator length to temperature variations is determined by the coefficient of thermal expansion (CTE) α_T, where k_T is defined as the temperature sensitivity of the normalized frequency shift. The temperature sensitivity k_T is determined by the TCDk and the CTE of the substrate from (6). By consulting the Rogers circuit materials manual, we know that Rogers RO3006, RO3010, and RO3210 have high TCDk, which is much larger than the CTE. Therefore, the temperature response of the sensor tag will be mainly contributed by the TCDk.

Temperature sensing simulations were performed using RO3006, RO3010, and RO3210 substrates, and the tag with a single bit was designed by adjusting the parameters as shown in Fig. 13. The three resonators use the same size, where $R = 14$ mm, ro = 9.25 mm, Gap = 1 mm, $D = 2$ mm, and $S = 2$ mm. For the substrate dielectric, the dielectric constant at room temperature is ε_r (20 °C). If the temperature increases, the dielectric constant decreases.

The value of the dielectric constant decrease for a temperature increase of 20 °C can be calculated by the following equation [24]:

$$\delta\varepsilon_r = \varepsilon_r \times TCDk \left(\frac{\text{ppm}}{^\circ\text{C}}\right) \times 20\ ^\circ\text{C}. \tag{7}$$

Table III shows the variation of the dielectric constant of the substrate when the temperature is varied from 0 °C to 100 °C.

According to the above analysis, the greater the TCDk, the greater the change in the dielectric constant and the better the sensitivity to temperature for the same degree of temperature increase, while the smaller the CTE, the less the resonant frequency is affected by the expansion of the substrate. According to the Rogers series product information, the selected substrates have very low water absorption and the effect of humidity on the substrate parameters can be ignored. The global variable ε_r is set in HFSS and the change in the dielectric constant is simulated by using the optimetrics function. The simulation outcomes are depicted in Fig. 14. RO3006 substrate simulation frequency results are 2.25–2.3 GHz, RO3010 substrate simulation frequency results are 2.73–2.8 GHz, and RO3210 substrate simulation frequency results are 3.67–3.74 GHz. According to a comparison of the frequency offset results, the frequency offset of the RO3006

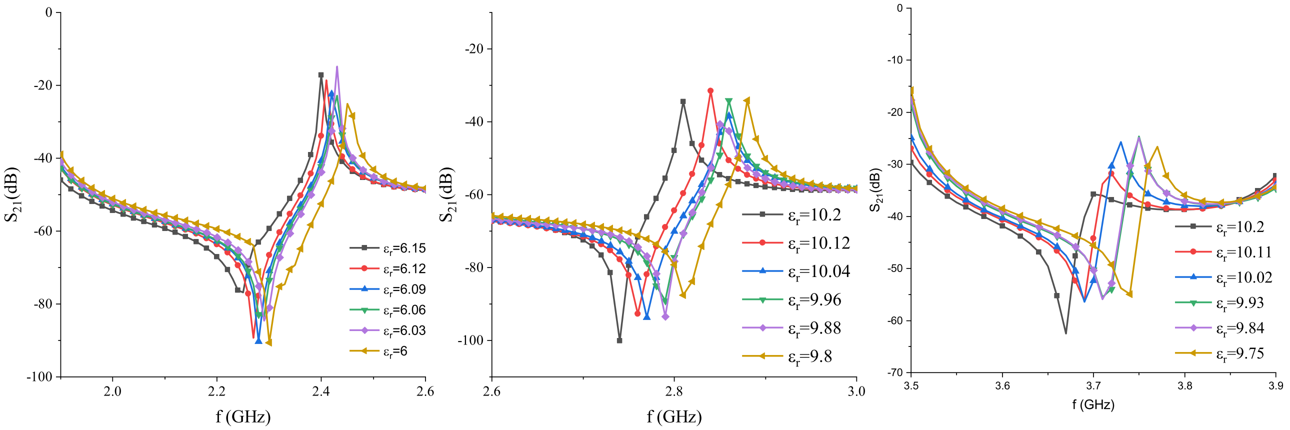

(a) (b) (c)

Fig. 14. Simulation results of the temperature sensing tag. (a) Tag for the RO3006 substrate. (b) Tag for the RO3010 substrate. (c) Tag for the RO3210 substrate.

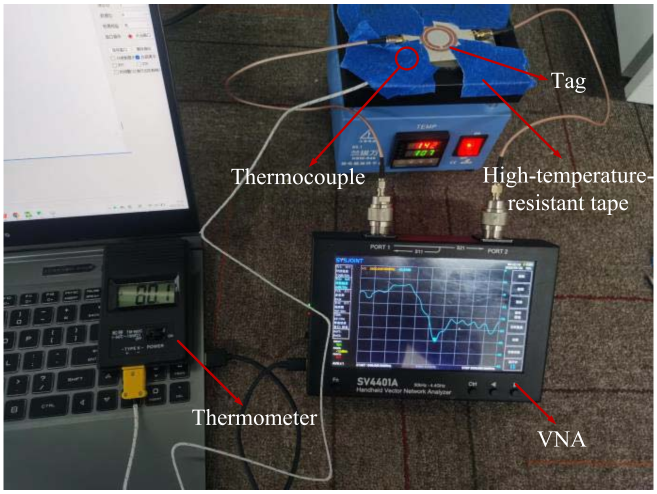

Fig. 15. Temperature detection experiment scene.

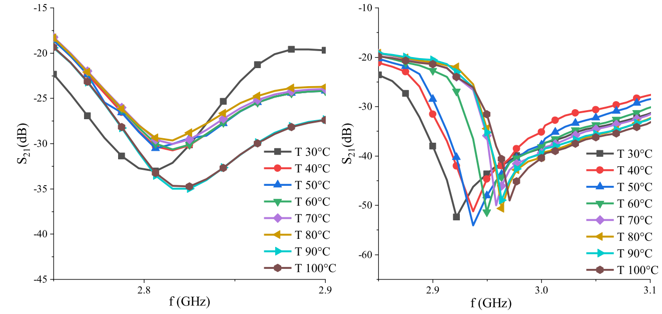

(a) (b)

Fig. 16. Actual tag temperature test results. (a) RO3006 tag test results. (b) RO3010 tag test results.

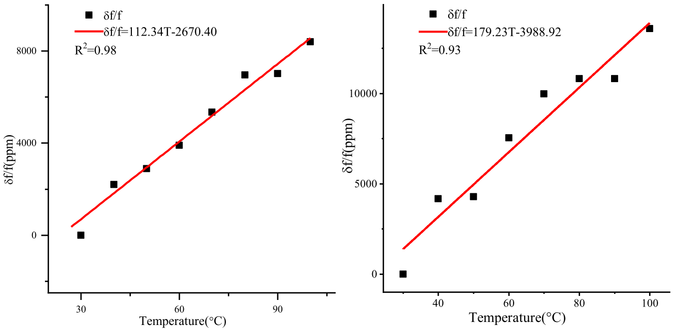

(a) (b)

Fig. 17. Fit relationship between the normalized resonant frequency shift of the antenna sensor and the temperature variation. (a) Fit curve of the measurement results of the RO3006 tag. (b) Fit curve of the measurement results of the RO3010 tag.

substrate is smaller, although the frequency offset results of the RO3010 and RO3210 substrates are comparable.

According to the laboratory circumstances, RO3006 and RO3010 substrates were chosen to build the tags, which were then experimentally tested using the method depicted in Fig. 15, in which the test sensors were placed on a heating table and secured with high-temperature-resistant tape. Due to the loss of heat transfer between the sensor and the heating table, to precisely detect the temperature change, a temperature measurement thermocouple adheres to the sensor surface with high-temperature-resistant tape to record the tag's temperature change in real time. The house's initial temperature was 30 °C. By adjusting the heating temperature of the heating table, the 30 °C–100 °C measurement range for the temperature experiment was determined. Fig. 16 demonstrates the detection outcomes of the RO3006 and RO3010 substrate tags.

The resonant frequency shifts at various temperatures are normalized to the sensor's resonant frequency. Fig. 17 depicts the relationship between the recorded normalized resonant frequency shift and temperature fluctuation. It can be seen that there is a good linear relationship between the frequency and temperature variation. Since the TCDk of the RO3006 substrate is relatively small, the frequency shift is smaller and the slope of the fit curve is smaller for the same change in temperature, which corresponds to the trend of the simulation findings. The fit curve of the RO3006 substrate is $df/f = 112.34T - 2670.40$ and the fit curve of RO3010 is $df/f =$

TABLE IV
COMPARISON OF THE PROPOSED SENSOR WITH PREVIOUS DESIGNS

Ref. No.	Application	Topology	Measurement type	Maximum sensing bandwidth	Operating frequency	Sensitivity K = df/dX
[25]	Discriminate different states of vanadium redox solutions	CSRR with a negative resistance compensation circuit	contact	170MHz	6GHz	2.3
[26]	Sensing chemical concentration	MTM-infused planar microwave sensor	contact	900MHz	2.6GHz	6.4
[27]	Sensing chemical concentration	SRR	contact	15MHz	1.19GHz	0.6
[28]	Detect changes in the real-relative permittivity of dielectric laminates	CSRRs couple to a splitter-combiner microstrip section	contact	2400MHz	4.2975GHz	6.4
[29]	Relative humidity level sensing	Two CSRR	contact	50MHz	5.15GHz	0.833
[30]	Water measurement	CSRR	contact	632MHz	2.2GHz	0.80
[31]	Detect the pH variation	SRR	contact	0.174MHz	2.2GHz	0.043
[32]	Environmental Temperature	CSRR	contact	550MHz	2.23GHz	5.5
This work	Detect the temperature variation	CSRR	contact	50MHz	2.9GHz	0.71
	Detect the humidity variation	CSRR	contact	90MHz		1.79

179.23T – 3988.92. By definition, the measured temperature sensitivity kT of RO3006 substrate is 112.34 ppm/°C and that of RO3010 substrate is 179.23 ppm/°C. The temperature sensor made by comparing the RO3010 substrate is more effective. Since the dielectric constant of the substrate changes with temperature, when the temperature returns to room temperature, the dielectric constant also returns to the initial state, so the temperature sensor made from this temperature-sensitive substrate can be reused to reduce the waste of resources.

Table IV compares the proposed temperature and humidity sensor with the existing literature on split-ring resonator (SRR) structured as well as planar microwave sensors in several aspects. The CSRR structured sensors are widely used, some widely used for liquid characterization, and can be either invasive, that is, the sensor is in direct contact with the material under test (MUT) [30], or noninvasive, that is, the sensor is not in direct contact with the MUT [25], [26], [27]. In addition, this type of sensor can be applied for the detection of the surrounding environment [28], [29], [31], [32]. However, their analysis is performed only on a single MUT. In this article, we propose a sensor that can be used for both temperature and humidity detection, and by consulting the Rogers series product manual, a temperature-sensitive substrate with low water absorption is selected for temperature detection and humidity detection is achieved by filling with PVA.

IV. CONCLUSION

In this study, we investigate the effect of each CSRR parameter on the simulation results and build a 5-bit tag based on the CSRR structure. The suggested tag enhances the number of bits by increasing the number of resonant rings, while parameter tweaking keeps the resonant frequency within the acceptable range. By covering a temperature-sensitive substrate with a humidity-sensitive substance, this study enables the sensor to perform multiparameter detection and conducts an experimental comparison analysis of the humidity sensor built with three substrates and the temperature sensor made with two substrates. According to the experimental measurement findings and the analysis of the normalized fitting data, the humidity sensitivity of the sensor is about 1.8 MHz/RH and the designed sensor is reversible and cost-effective.

This article's drawback is that the thickness and form of the PVA cannot be altered to investigate the sensitivity of substrate characteristics to humidity detection.

REFERENCES

[1] K. V. S. Rao, P. V. Nikitin, and S. F. Lam, "Antenna design for UHF RFID tags: A review and a practical application," *IEEE Trans. Antennas Propag.*, vol. 53, no. 12, pp. 3870–3876, Dec. 2005, doi: 10.1109/TAP.2005.859919.

[2] A. M. J. Marindra and G. Y. Tian, "Chipless RFID sensor tag for metal crack detection and characterization," *IEEE Trans. Microw. Theory Techn.*, vol. 66, no. 5, pp. 2452–2462, May 2018, doi: 10.1109/TMTT.2017.2786696.

[3] J. Yeo, J.-I. Lee, and Y. Kwon, "Humidity-sensing chipless RFID tag with enhanced sensitivity using an interdigital capacitor structure," *Sensors*, vol. 21, no. 19, p. 6550, Sep. 2021, doi: 10.3390/s21196550.

[4] L. Liu and L. Chen, "Characteristic analysis of a chipless RFID sensor based on multi-parameter sensing and an intelligent detection method," *Sensors*, vol. 22, no. 16, p. 6027, Jan. 2022, doi: 10.3390/s22166027.

[5] N. Javed, M. A. Azam, and Y. Amin, "Chipless RFID multisensor for temperature sensing and crack monitoring in an IoT environment," *IEEE Sensors Lett.*, vol. 5, no. 6, pp. 1–4, Jun. 2021, doi: 10.1109/LSENS.2021.3083218.

[6] J. W. Sanders, J. Yao, and H. Huang, "Microstrip patch antenna temperature sensor," *IEEE Sensors J.*, vol. 15, no. 9, pp. 5312–5319, Sep. 2015, doi: 10.1109/JSEN.2015.2437884.

[7] J. Anum Satti et al., "Miniaturized humidity and temperature sensing RFID enabled tags," *Int. J. RF Microw. Comput.-Aided Eng.*, vol. 28, no. 1, Jul. 2017, Art. no. e21151, doi: 10.1002/mmce.21151.

[8] E. M. Amin, N. C. Karmakar, and B. W. Jensen, "Fully printable chipless RFID multi-parameter sensor," *Sens. Actuators A, Phys.*, vol. 248, pp. 223–232, Sep. 2016, doi: 10.1016/j.sna.2016.06.014.

[9] M. Linek, "Low-shrink airfield cement concrete with respect to thermal resistance," in *Proc. MATEC Web Conf.*, vol. 133, Jan. 2017, p. 7002, doi: 10.1051/matecconf/201713307002.

[10] T. Athauda and N. C. Karmakar, "The realization of chipless RFID resonator for multiple physical parameter sensing," *IEEE Internet Things J.*, vol. 6, no. 3, pp. 5387–5396, Jun. 2019, doi: 10.1109/JIOT.2019.2901470.

[11] A. Chauhan and U. K. Sharma, "Influence of temperature and relative humidity variations on non-uniform corrosion of reinforced concrete," *Structures*, vol. 19, pp. 296–308, Jun. 2019, doi: 10.1016/j.istruc.2019.01.016.

[12] S. Ahmad, N. Khalid, and R. Mirzavand, "Detection of soil moisture, humidity, and liquid level using CPW-based interdigital capacitive sensor," *IEEE Sensors J.*, vol. 22, no. 11, pp. 10338–10345, Jun. 2022, doi: 10.1109/JSEN.2022.3167337.

[13] C. Jia et al., "A novel differential capacitive humidity sensor on SIW re-entrant cavity microwave resonators with PEDOT:PSS film," *IEEE Sensors J.*, vol. 22, no. 7, pp. 6576–6585, Apr. 2022, doi: 10.1109/JSEN.2022.3155235.

[14] Z. R. M. Hajiyat, A. Ismail, A. Sali, and M. N. Hamidon, "Antenna in 6G wireless communication system: Specifications, challenges, and research directions," *Optik*, vol. 231, Apr. 2021, Art. no. 166415, doi: 10.1016/j.ijleo.2021.166415.

[15] L. Wang et al., "Wideband dual-polarized binary coding antenna with wide beamwidth and its array for millimeter-wave applications," *IEEE Antennas Wireless Propag. Lett.*, vol. 19, no. 4, pp. 636–640, Apr. 2020, doi: 10.1109/LAWP.2020.2974160.

[16] B. R. Behera and P. Suraj, "Effect of substrates on metamaterial based antenna design and analysis of antenna using different substrates," in *Proc. Int. Conf. Wireless Commun., Signal Process. Netw. (WiSPNET)*, Mar. 2016, pp. 665–669, doi: 10.1109/WiSPNET.2016.7566216.

[17] C. Saha and J. Y. Siddiqui, "A comparative analysis for split ring resonators of different geometrical shapes," in *Proc. IEEE Appl. Electromagn. Conf. (AEMC)*, Dec. 2011, pp. 1–4, doi: 10.1109/AEMC.2011.6256871.

[18] M. E. B. Jalil et al., "High capacity and miniaturized flexible chipless RFID tag using modified complementary split ring resonator," *IEEE Access*, vol. 9, pp. 33929–33943, 2021, doi: 10.1109/ACCESS.2021.3061792.

[19] E. M. Amin, C. Nemai Karmakar, and B. Winther-Jensen, "Polyvinylalcohol (PVA)-based RF humidity sensor in microwave frequency," *Prog. Electromagn. Res. B*, vol. 54, pp. 149–166, 2013, doi: 10.2528/PIERB13061716.

[20] G. Marchi, V. Mulloni, M. Manekiya, M. Donelli, and L. Lorenzelli, "A preliminary microwave frequency characterization of a nafion-based chipless sensor for humidity monitoring," in *Proc. IEEE SENSORS*, Oct. 2020, pp. 1–4, doi: 10.1109/SENSORS47125.2020.9278752.

[21] A. Awadhia, S. Patel, and S. Agrawal, "Dielectric investigations in PVA based gel electrolytes," *Prog. Crystal Growth Characterization Mater.*, vol. 52, nos. 1–2, pp. 61–68, Mar. 2006, doi: 10.1016/j.pcrysgrow.2006.03.009.

[22] M. K. Mohanapriya, K. Deshmukh, M. B. Ahamed, K. Chidambaram, and S. K. K. Pasha, "Influence of cerium oxide (CeO_2) nanoparticles on the structural, morphological, mechanical and dielectric properties of PVA/PPy blend nanocomposites," *Mater. Today, Proc.*, vol. 3, no. 6, pp. 1864–1873, 2016, doi: 10.1016/j.matpr.2016.04.086.

[23] J. Yao, F. M. Tchafa, A. Jain, S. Tjuatja, and H. Huang, "Far-field interrogation of microstrip patch antenna for temperature sensing without electronics," *IEEE Sensors J.*, vol. 16, no. 19, pp. 7053–7060, Oct. 2016, doi: 10.1109/JSEN.2016.2597739.

[24] K. Carver and J. Mink, "Microstrip antenna technology," *IEEE Trans. Antennas Propag.*, vol. AP-29, no. 1, pp. 2–24, Jan. 1981, doi: 10.1109/TAP.1981.1142523.

[25] N. Kazemi, K. Schofield, and P. Musilek, "A high-resolution reflective microwave planar sensor for sensing of vanadium electrolyte," *Sensors*, vol. 21, no. 11, p. 3759, Jan. 2021, doi: 10.3390/s21113759.

[26] M. Abdolrazzaghi, M. Daneshmand, and A. K. Iyer, "Strongly enhanced sensitivity in planar microwave sensors based on metamaterial coupling," *IEEE Trans. Microw. Theory Techn.*, vol. 66, no. 4, pp. 1843–1855, Apr. 2018, doi: 10.1109/TMTT.2018.2791942.

[27] N. Kazemi, M. Abdolrazzaghi, and P. Musilek, "Comparative analysis of machine learning techniques for temperature compensation in microwave sensors," *IEEE Trans. Microw. Theory Techn.*, vol. 69, no. 9, pp. 4223–4236, Sep. 2021, doi: 10.1109/TMTT.2021.3081119.

[28] A. M. Albishi, M. K. E. Badawe, V. Nayyeri, and O. M. Ramahi, "Enhancing the sensitivity of dielectric sensors with multiple coupled complementary split-ring resonators," *IEEE Trans. Microw. Theory Techn.*, vol. 68, no. 10, pp. 4340–4347, Oct. 2020, doi: 10.1109/TMTT.2020.3002996.

[29] M. Abdolrazzaghi, F. Hariri, M. Chu, H. Naguib, and M. Daneshmand, "Relative humidity sensing using PANI/PVA integrated with feedback oscillator circuit," in *Proc. IEEE SENSORS*, Oct. 2019, pp. 1–4, doi: 10.1109/SENSORS43011.2019.8956563.

[30] B.-X. Wang, W.-S. Zhao, D.-W. Wang, J. Wang, W. Li, and J. Liu, "Optimal design of planar microwave microfluidic sensors based on deep reinforcement learning," *IEEE Sensors J.*, vol. 21, no. 24, pp. 27441–27449, Dec. 2021, doi: 10.1109/JSEN.2021.3124294.

[31] Z. Abbasi, H. Niazi, M. Abdolrazzaghi, W. Chen, and M. Daneshmand, "Monitoring pH level using high-resolution microwave sensor for mitigation of stress corrosion cracking in steel pipelines," *IEEE Sensors J.*, vol. 20, no. 13, pp. 7033–7043, Jul. 2020, doi: 10.1109/JSEN.2020.2978086.

[32] W.-J. Wu, W.-S. Zhao, D.-W. Wang, B. Yuan, and G. Wang, "A temperature-compensated differential microstrip sensor for microfluidic applications," *IEEE Sensors J.*, vol. 21, no. 21, pp. 24075–24083, Nov. 2021, doi: 10.1109/JSEN.2021.3115570.

Lei Kang received the B.S. degree in electrical engineering and its automation from Hebei University, Baoding, China, in 2019. She is currently pursuing the master's degree in control science and engineering with the Shanghai Institute of Technology University, Shanghai, China.

Her current research interests include multiparameter sensor design-based radio-frequency identifier (RFID) detection systems and structural health monitoring.

Lan Chen received the M.S. degree in signal and information processing from Tongji University, Shanghai, China, in 2004, and the Ph.D. degree in astronomical technology and method science from the Shanghai Astronomical Observatory, Chinese Academy of Sciences, Shanghai, in 2010.

She is currently a Professor with the Shanghai Institute of Technology, Shanghai, where she is also the Associate Dean of the School of Electrical and Electronic Engineering. Her current research interests include high-speed digital signal processing, digital terminal technology research, and signal simulation technology.

Luyi Liu received the B.S. degree in electrical engineering and its automation from the Shanghai University of Electric Power, Shanghai, China, in 2020. He is currently pursuing the master's degree in control science and engineering with the Shanghai Institute of Technology University, Shanghai.

His current research interests include multiparameter sensor design based on radio-frequency identifier (RFID) detection systems, reconfigurable antenna design, and wireless sensor networks.

Zhichong Wan received the B.E. degree in electronic information engineering from Nanchang University, Nanchang, China, in 2019. He is currently pursuing the master's degree in control science and engineering with the Shanghai Institute of Technology, Shanghai, China.

His current research interests include machine learning and embedded development.

Guochun Wan received the M.S. and Ph.D. degrees in transportation information engineering and control from Tongji University, Shanghai, China, in 2005 and 2011, respectively.

He became an Associate Professor in 2002. He joined the Department of Electronic Science and Technology, Tongji University, in 2006. His current research interests include signal and information processing, with an emphasis on error-correcting coding, Very Large Scale Integration (VLSI) architectures, radio-frequency identifier (RFID) strain sensor and system-on-chip (SoC) design for communications, and coding theory applications.

Liyu Xie received the B.S. and M.S. degrees in mechanical engineering from Tongji University, Shanghai, China, in 2000 and 2003, respectively, and the Ph.D. degree in system design engineering from Keio University, Tokyo, Japan, in 2009.

In 2019, he became an Associate Professor at the College of Civil Engineering, Tongji University. His current research interests include smart sensors, structural health monitoring, and structural vibration control.